

This document is confidential and is proprietary to the American Chemical Society and its authors. Do not copy or disclose without written permission. If you have received this item in error, notify the sender and delete all copies.

Exfoliation of Graphite into Graphene in Aqueous Solutions of Inorganic Salts

Journal:	<i>Journal of the American Chemical Society</i>
Manuscript ID:	ja-2014-017156.R1
Manuscript Type:	Article
Date Submitted by the Author:	27-Mar-2014
Complete List of Authors:	Parvez, Khaled; Max Planck Institute for Polymer Research, Wu, Zhong-Shuai; Max Planck Institute for Polymer Research, Li, Rongjin; Max Planck Institute for Polymer Research, Liu, Xianjie; Linköping University, Graf, Robert; Max Planck Institute for Polymer Research, Feng, Xinliang; Max Planck Institute for Polymer Research, Müllen, Klaus; Max-Planck-Institute for Polymer Research,

SCHOLARONE™
Manuscripts

Exfoliation of Graphite into Graphene in Aqueous Solutions of Inorganic Salts

Khaled Parvez,[†] Zhong-Shuai Wu,[†] Rongjin Li,[†] Xianjie Liu,[‡] Robert Graf,[†] Xinliang Feng,^{†,§,}*

Klaus Müllen^{†,}*

[†]Max Planck Institute for Polymer Research, Ackermannweg 10, Mainz 55128, Germany

[‡]Department of Physics, Chemistry and Biology, Linköping University, SE-58183 Linköping, Sweden

[§]School of Chemistry and Chemical Engineering, Shanghai Jiao Tong University, 200240 Shanghai, P. R. China

*Address correspondence to muellen@mpip-mainz.mpg.de; feng@mpip-mainz.mpg.de

ABSTRACT:

Mass production of high-quality graphene sheets is essential for their practical application in electronics, optoelectronics, composite materials and energy-storage devices. Here we report a prompt electrochemical exfoliation of graphene sheets into aqueous solutions of different inorganic salts ((NH₄)₂SO₄, Na₂SO₄, K₂SO₄, etc). Exfoliation in these electrolytes leads to graphene with a high yield (>85%, ≤3 layers), large lateral size (up to 44 μm), low oxidation degree (a C/O ratio of 17.2), and a remarkable hole mobility of 310 cm² V⁻¹ s⁻¹. Further, highly conductive graphene films (11 Ω sq.⁻¹) are readily fabricated on an A4-size paper by applying brush painting of a concentrated graphene ink (10 mg/mL, in N,N'-dimethylformamide (DMF)).

1
2
3 All-solid-state flexible supercapacitors manufactured based on such graphene films deliver a
4 high area capacitance of 11.3 mF cm^{-2} and an excellent rate capability of 5000 mV s^{-1} . The
5 described electrochemical exfoliation shows great promise for the industrial-scale synthesis of
6 high-quality graphene for numerous advanced applications.
7
8
9

10
11
12
13 **KEYWORDS:** electrochemical exfoliation, high-quality graphene, electrolyte, graphene-ink,
14 supercapacitor
15
16

17 18 19 INTRODUCTION

20
21 Graphene, a two-dimensional honeycomb sp^2 carbon lattice, has received immense attention
22 for its potential application in next-generation electronic devices,^{1,2} composite materials,^{3,4}
23 energy storage devices,⁵ etc., due to its intriguing electrical, mechanical, and chemical
24 properties.^{6,7} Mass production of high-quality, solution-processable graphene *via* a simple low-
25 cost method, however, remains a major challenge. Several graphene preparation methods have
26 been developed since its discovery.⁸ Among them, mechanically exfoliated and epitaxially
27 grown graphene provides high-quality material, but in only limited quantities, for fundamental
28 research^{8,9}. Chemical vapour deposition (CVD) using catalytic metal substrates such as Ni or Cu,
29 produces large-area high-quality graphene.^{9,10} The major obstacles to cost-effective industrial-
30 scale production of CVD-grown graphene, however, are the requirements of high temperature, a
31 sacrificial metal, and multi-step transfer processes onto the desired substrates. Chemical
32 exfoliation of graphite based on the Hummers method is an appealing route to produce solution-
33 processable graphene oxide (GO) in bulk-scale, but requires thermal or chemical reduction to
34 partially restore the electronic properties of graphene.¹¹ Several other methods have been
35 developed to overcome these limitations, such as solvent- and/or surfactant-assisted liquid-phase
36 exfoliation,¹² electrochemical expansion,¹³ and formation of graphite intercalated compounds.¹⁴
37
38
39
40
41
42
43
44
45
46
47
48
49
50
51
52
53
54
55
56
57
58
59
60

1
2
3 Nevertheless, extensive sonication processes are indispensable for these methods, which limit the
4 size and yield of thin graphene layers.
5
6

7
8 Recently, electrochemical exfoliation of graphite has attracted attention due to its easy, fast,
9 and environmentally friendly nature to produce high-quality graphene.¹⁵⁻¹⁸ Electrochemical
10 exfoliation of graphite has been performed mainly in two different types of electrolytes, *i.e.*,
11 ionic-liquids^{17,19} and aqueous acids (*e.g.*, H₂SO₄ or H₃PO₄).^{15,18,20} Exfoliation in ionic liquids
12 results in only a low yield of graphene with a small lateral size (<5 μm), and is often
13 functionalised with the ionic liquids, which disrupt the electronic properties of graphene.^{17,21} On
14 the other hand, exfoliation in acidic electrolytes can yield graphene with a better quality and a
15 larger lateral size, but a significant amount of oxygen-containing functional groups cannot be
16 avoided due to the over-oxidation of graphite by the acid.^{15,18,20} Therefore, a proper electrolyte
17 system that can balance the high-quality and large-quantity synthesis of exfoliated graphene (EG)
18 is highly in demand.
19
20
21
22
23
24
25
26
27
28
29
30
31
32

33
34 In this work, we demonstrate a highly efficient electrochemical exfoliation of graphite in
35 aqueous inorganic salts, such as ammonium sulphate ((NH₄)₂SO₄), sodium sulphate (Na₂SO₄),
36 and potassium sulphate (K₂SO₄). Under neutral pH conditions for electrochemical exfoliation,
37 graphene sheets with the highest C/O ratio of 17.2 (*i.e.*, oxygen content of 5.5 atomic% [at%])
38 and lowest defect density were obtained. The EG sheets were readily produced on a scale of tens
39 of grams, with ~80% of the flakes larger than 5 μm, and ~85% of flakes having 1 to 3 layers.
40 Moreover, single-layer graphene sheets had a high hole mobility of 310 cm² V⁻¹ s⁻¹ with a sheet
41 resistance of 1.96 kΩ sq.⁻¹, which is superior to the chemically reduced graphene oxide (rGO).
42 The high solution-processability of EG further allowed for the preparation of concentrated
43 graphene ink in *N,N'*-dimethylformamide (DMF) without any additional surfactants. A simple
44
45
46
47
48
49
50
51
52
53
54
55
56
57
58
59
60

1
2
3 paintbrush application of EG-ink to A4-sized paper yielded highly conductive ($\sim 11 \Omega \text{ sq.}^{-1}$ with
4
5 0.74 mg cm^{-2} EG loading), mechanically stable, and large-area graphene films. All-solid-state
6
7 flexible supercapacitors fabricated based on such graphene paper exhibited a high-area capacity
8
9 of 11.3 mF cm^{-2} (at a scan rate of 1 mV s^{-1}) and a high rate capability (up to 5000 mV s^{-1}).
10
11

12 RESULTS AND DISCUSSION

13
14 **Graphene preparation by electrochemical exfoliation.** Electrochemical exfoliation of graphite
15
16 was performed in a two-electrode system using platinum as the counter electrode and a graphite
17
18 flake as the working electrode. Different types of aqueous inorganic salt electrolyte solutions
19
20 were examined and among them sulphate-containing salts such as $(\text{NH}_4)_2\text{SO}_4$ exhibited the best
21
22 exfoliation efficiency. Electrolyte solutions were prepared by dissolving $(\text{NH}_4)_2\text{SO}_4$ in water
23
24 (concentration of 0.1 M and pH ~ 6.5 -7.0). When a direct current (DC) voltage of +10 V was
25
26 applied to a graphite electrode, the graphite flakes began to dissociate and disperse into the
27
28 electrolyte solution (Fig. 1a). The voltage was kept constant for 3 to 5 min to complete the
29
30 exfoliation process. Afterwards, the exfoliated product was collected by vacuum filtration and
31
32 repeatedly washed with water to remove any residual salts. The yield of the exfoliated EG flakes
33
34 was more than 75% relative to the total weight of the starting graphite electrode. The collected
35
36 powder was then dispersed in DMF by sonication for 10 min. Thus, a dispersion of $\sim 2.5 \text{ mg/mL}$
37
38 was obtained, which was stable for 3 weeks without apparent agglomeration (Fig. 1b).
39
40 Remarkably, the exfoliation process could be readily scaled up depending on the type and size of
41
42 the graphite electrode used (Fig. S1). For example, in a series of electrochemical experiments,
43
44 $\sim 16.3 \text{ g}$ of graphene sheets was obtained (Fig. 1c) within 30 min using three graphite foils (each
45
46 with a dimension of $11.5 \text{ cm} \times 2.5 \text{ cm}$) simultaneously (Fig. S1a).
47
48
49
50
51
52
53
54
55
56
57
58
59
60

1
2
3 In addition to $(\text{NH}_4)_2\text{SO}_4$, various aqueous electrolyte solutions of inorganic salts, such as
4 NH_4Cl , Na_2SO_4 , NaNO_3 , K_2SO_4 , and NaClO_4 were examined in the electrochemical exfoliation
5 process (see Fig. S2-S3 and Table S1 for details). Salts containing anions, such as ClO_4^- , Cl^- , and
6 NO_3^- , had no apparent exfoliation effects. Expansion of the graphite electrode was only observed
7 when using ClO_4^- and NO_3^- anions. In contrast, salts containing sulphate anions (*e.g.*, SO_4^{2-})
8 exhibited pronounced exfoliation efficiency. Thin graphene sheets were readily obtained in less
9 than 5 min (Fig. S2d,e and Fig. S3). The superior exfoliation efficiency of sulphate salts
10 compared to other anions can be attributed to the lower reduction potential of SO_4^{2-} (+0.20 V) to
11 generate SO_2 gas. In contrast, the reduction potential of ClO_4^- and NO_3^- ions to produce Cl_2 and
12 NO gases is as high as 1.42 and 0.96 V, respectively (see Scheme S1 for details).
13
14
15
16
17
18
19
20
21
22
23
24
25
26

27 We propose the mechanism of electrochemical exfoliation depicted in Fig. 1d: (i) Applying
28 bias voltage results in a reduction of water at the cathode, creating hydroxyl ions (OH^-) that act
29 as a strong nucleophile in the electrolyte. The nucleophilic attack of graphite by OH^- ions
30 initially occurs at the edge sites and grain boundaries. (ii) Oxidation at the edge sites and grain
31 boundaries then leads to depolarization and expansion of the graphite layers, thereby facilitating
32 the intercalation of sulphate ions (SO_4^{2-}) within the graphitic layers. During this stage, water
33 molecules may co-intercalate with the SO_4^{2-} anions. (iii) Reduction of SO_4^{2-} anions and self-
34 oxidation of water produce gaseous species such as SO_2 , O_2 , and others, as evidenced by the
35 vigorous gas evolution during the electrochemical process.^{22,23} These gaseous species can exert
36 large forces on the graphite layers, which are sufficient to separate weakly bonded graphite
37 layers from one another.²⁴ This hypothesis was confirmed by controlled experiments in which a
38 constant bias voltage (*e.g.*, +10 V) was applied to graphite electrodes for different time periods
39 (5 to 60 s), and changes in the morphology of the graphite foil were monitored by scanning
40
41
42
43
44
45
46
47
48
49
50
51
52
53
54
55
56
57
58
59
60

1
2
3 electron microscopy (SEM) and optical microscopy. SEM images of both the surface and edge of
4 the original graphite show closely packed layers (Fig. 2a-c). When voltage was applied, however,
5 the surface and edge morphology changed drastically within a few seconds (Fig. S4). After
6 applying voltage for 5 s, the edge of the graphite foil expanded and the cracks in the graphite
7 layers increased (Fig. S5b and c). When the time was increased from 5 to 60 s, a large amount of
8 graphene flakes was exfoliated and dispersed into the electrolyte solution. After 60 s, the edge of
9 the graphite foil expanded to almost 10 times that in the initial state (Fig. 2b, h). Moreover, a
10 network of ripples on the surface of the graphite was clearly identified in the SEM images (Fig.
11 2d,g and Fig. S5a,d), which might be due to the visible gas evolution causing expansion and
12 swelling of the graphite layers. These observations strongly support our hypothesis that during
13 the electrochemical process, edge and grain boundaries of the graphite electrode open up first,
14 which facilitates anion intercalation and results in exfoliated graphene sheets. A detailed reaction
15 mechanism on the oxidation, *i.e.*, oxide bond formation of graphite, is proposed and discussed in
16 the Supplementary Information (Scheme S2).
17
18
19
20
21
22
23
24
25
26
27
28
29
30
31
32
33
34
35

36 We further investigated the effect of the electrolyte concentration on the applied potential
37 for graphite exfoliation. The voltage or potential for graphite exfoliation decreased upon
38 increasing the concentration of $(\text{NH}_4)_2\text{SO}_4$ (Fig. S6a). When the concentration of $(\text{NH}_4)_2\text{SO}_4$ was
39 lower than 0.01 M, the yield of EG was less than 5 wt%, indicating a limited amount of ions
40 available for graphite intercalation. In sharp contrast, when the concentration increased from
41 0.01 to 1.0 M, a high yield of EG (> 75 wt%) was obtained. A further increase in the
42 concentration (*e.g.*, 3.0 and 5.0 M), however, failed to enhance the graphene yield (< 50%, Fig.
43 S6b). As discussed above, the initial oxidation of graphite by OH^- ions at the edge and/or grain
44 boundaries is essential for the depolarization and expansion of the graphite layers as well as for
45
46
47
48
49
50
51
52
53
54
55
56
57
58
59
60

1
2
3 the following anion intercalation. With the high concentration of $(\text{NH}_4)_2\text{SO}_4$, the formation of
4
5 OH^- ions is suppressed due to the low water content, therefore, the graphite edge oxidation,
6
7 expansion, and SO_4^{2-} ion intercalation processes are expected to be relatively slow.
8
9

10 **Morphological and structural characterizations of EG.** The morphology of the EG sheets was
11 investigated by SEM and atomic force microscopy (AFM). EG nanosheets were deposited on
12 SiO_2 substrates using the Langmuir-Blodgett technique (Fig. S7a). Figure 3a shows a SEM
13 image of a typical EG sheet ($18.7 \mu\text{m}$). Lateral size measurements of 120 EG sheets reveal that
14
15 over 80% of the EG sheets are larger than $5.0 \mu\text{m}$ (Fig. 3b), and the largest flake size observed is
16
17 $\sim 44.0 \mu\text{m}$ (Fig. S7b). A histogram of flake thickness acquired across EG flakes using AFM
18
19 shows a mean thickness of $\sim 0.72 \text{ nm}$ (Fig. 3c), confirming the monolayer nature, which is
20
21 comparable with the thickness of pristine graphene on a Si wafer²⁵. The measured thickness of a
22
23 bilayer and a multi-layer (≥ 4 layers) EG is 1.30 and 3.11 nm, respectively (Fig. S8). The
24
25 thickness distribution of more than 50 sheets calculated from the AFM height profile is presented
26
27 in Fig. 3d. Remarkably, more than 85% of EG nanosheets comprises thin graphene (≤ 3 layers),
28
29 where single and bi-layer graphenes are the dominant products (together $\sim 72\%$). High-
30
31 resolution transmission electron microscopic (HRTEM) images further disclose that the EG
32
33 sheets range from a single layer to four layers (Fig. 3e and S9). The selected area electron
34
35 diffraction (SAED) pattern in Figure 3f exhibits a typical six-fold symmetric diffraction with
36
37 stronger diffraction from (1-210) plane than from the (0-110) plane, indicating the high
38
39 crystallinity of a bilayer graphene sheet.^{13,26}
40
41
42
43
44
45
46
47
48
49

50 We then used Raman spectroscopy to identify defects in the graphene^{27,28}. We performed
51 Raman spectroscopy and mapping with a 532-nm excitation laser on EG deposited on SiO_2/Si
52
53 substrates. Raman mapping of D and G peaks from a few layer EG sheet (2 - 4 layers; selected
54
55
56
57
58
59
60

1
2
3 layers are shown in Fig. 4a) was extracted and plotted in Fig. 3b and c, respectively. The D peak
4 (~ 1350 cm^{-1}) was caused by the breathing mode of the sp^2 carbon atoms and activated by the
5
6 existence of defects such as edges, functional groups, or structural disorders²⁹. The intensity
7
8 contrast in the colour scale in Fig. 4b and c shows that the intensity of the G peak is more than
9
10 two times that of D peak (mean I_D/I_G ratio = 0.42), indicating a low degree of defects. The
11
12 corresponding Raman spectra in Fig. 4d (measured near the centre of the graphene flake)
13
14 demonstrates an I_D/I_G ratio of 0.25, which is much smaller than for chemically or thermally
15
16 reduced GO (~1.1 to 1.5)³⁰, and electrochemically exfoliated graphene (0.4) in acidic solution¹⁵.
17
18
19
20
21

22 X-ray photoelectron spectroscopy (XPS) was used to probe the chemical composition of the
23
24 as-prepared EG. The EG showed approximately 5.5 at% oxygen content on graphene (Fig. S10),
25
26 which was much lower than that obtained in acidic electrolyte solution (*i.e.*, 7.5 at%).¹⁵ Despite
27
28 the presence of a tiny amount of oxygen originating from the oxidation of graphite by OH^- ions
29
30 during the electrochemical process, the C/O ratio of 17.2 for EG was significantly higher than
31
32 those reported for EG and rGO.^{15,31,32} A detailed comparison of the C/O ratios between rGO and
33
34 different types of exfoliated graphene is presented in Table S2. The deconvoluted XPS spectra of
35
36 the C1s peak (Fig. 5a) disclose the presence of 3.64 at% of C-OH (285.5 eV), 0.38 at% of C=O
37
38 (287.6 eV), and 1.48 at% of C(O)-O (290.1 eV) groups.
39
40
41
42

43 Further structural analysis of EG by ^{13}C magic angle spinning (MAS) NMR revealed a
44
45 broad signal centred at 122 ppm (graphitic, C sp^2), indicating the presence of pure sp^2 hybridised
46
47 carbon sites (Fig. S11). In contrast, the NMR spectrum of GO showed an additional signal of sp^3
48
49 hybridised carbons bound to oxygen (C-OH or C-O-C) in the range of 60 to 70 ppm. The signal
50
51 of EG at 122 ppm was quite broad when compared to that of GO. This can be attributed to the
52
53 high conductivity of EG, resulting in a higher number of perturbing magnetic moments of the
54
55
56
57
58
59
60

1
2
3 free charges. The spinning of the EG sample in the magnetic field was difficult because of the
4
5 high conductivity, which also limited the filling of MAS rotors.
6
7

8 The powder X-ray diffraction pattern of EG displayed a peak at 26.3° (d -spacing 3.48 Å;
9 Fig. S12). The presence of a small amount of functional groups in EG acts as a spacer between
10 layers and results in a lower 2θ angle with large d -spacing compared to graphite (26.5° , d -
11 spacing ~ 3.36 Å), but significantly higher than rGO (25.0° , d -spacing ~ 3.56 Å).³¹ Figure 5b
12 displays the ultraviolet photoelectron spectra around the secondary-electron threshold region for
13 a thin film of EG. The measured work function (Φ_{EG}) of EG was 4.57 eV, slightly higher than
14 that of pristine graphene (~ 4.50 eV).³³ This can be attributed to the presence of oxygen-
15 containing functional groups in EG that can produce surface dipoles via the extraction of π
16 electrons from graphene.³⁴
17
18
19
20
21
22
23
24
25
26
27
28

29 **Electronic properties of EG.** To examine the electronic properties of the as-prepared EG flakes,
30 we fabricated field-effect transistor (FET) devices based on thin EG film (thickness $\sim 0.7 - 4$ nm)
31 and a single-layer EG sheet (thickness ~ 0.71 nm), respectively (Fig. S13). Both thin EG film and
32 isolated single-layer EG on SiO_2/Si substrates were prepared by using the Langmuir-Blodgett
33 technique. The detailed device fabrication is described in the experimental section. The transfer
34 curves of the FET devices based on thin EG film and single-layer EG are presented in Fig. 6a
35 and c, respectively. Notably, the device based on thin EG film (Fig. 6a,b) possesses a maximum
36 hole mobility of $98.2 \text{ cm}^2 \text{ V}^{-1} \text{ s}^{-1}$, whereas single-layer EG (Fig. 6c) gives an excellent hole
37 mobility of $\sim 310 \text{ cm}^2 \text{ V}^{-1} \text{ s}^{-1}$ and a sheet resistance of $1.96 \text{ k}\Omega \text{ sq.}^{-1}$ (Fig. 6d), comparable with un-
38 doped CVD-grown graphene ($1.05 \text{ k}\Omega \text{ sq.}^{-1}$)³⁵. The lower mobility of the thin film device can be
39 attributed to the interjunction resistance between EG flakes. It should be emphasised that the
40 hole mobility of single-layer EG achieved in this work is significantly higher than that of
41
42
43
44
45
46
47
48
49
50
51
52
53
54
55
56
57
58
59
60

1
2
3 chemically reduced GO ($123 \text{ cm}^2 \text{ V}^{-1} \text{ s}^{-1}$)³¹ or electrochemically exfoliated graphene in acidic
4 solution ($233 \text{ cm}^2 \text{ V}^{-1} \text{ s}^{-1}$)¹⁵ (see Table S3 for detailed comparison).
5
6

7
8 **EG thin films on plastic substrate.** The high-quality and solution-processability of EG allow
9 for fabricating transparent graphene films on flexible polyethylene terephthalate (PET) substrates
10 by a vacuum filtration and dry transfer method (Fig. S14a).¹⁵ Briefly, an EG dispersion of 0.1
11 mg/mL in DMF was vacuum-filtered through a polytetrafluoroethylene (PTFE) membrane
12 followed by mechanically pressing the filtered film against a PET substrate. Afterwards, the
13 PTFE membrane was peeled off, leaving the transferred EG film on the substrate due to van der
14 Waals interaction between the substrate and graphene. The thickness of the transferred EG film
15 could be adjusted by controlling the filtration volume and the concentration of EG dispersions.
16 For example, vacuum filtration of 3 and 9 mL of EG dispersions resulted in ~6.0 and ~16.0 nm
17 graphene films on PET with ~91% and ~80% transparency, respectively (Fig. S14b). The sheet
18 resistance (R_s) measured by a four-point probe system revealed a mean value of 24.2 and 7.56
19 $\text{k}\Omega \text{ sq.}^{-1}$ for 6.0 and 16.0 nm films, respectively. Low temperature annealing (*i.e.*, 300°C) of the
20 EG films decreased the R_s to 7.61 and 1.81 $\text{k}\Omega \text{ sq.}^{-1}$, respectively (Fig. S14c). Remarkably,
21 further doping the EG films with 65% HNO_3 for 2 h led to R_s values of 0.87 and 0.33 $\text{k}\Omega \text{ sq.}^{-1}$,
22 respectively, without sacrificing the original transparency (Fig. S15).
23
24
25
26
27
28
29
30
31
32
33
34
35
36
37
38
39
40
41
42
43

44 **EG ink-coated paper for flexible supercapacitors.** We further demonstrated the use of EG as
45 conductive ink, which is an important requirement for next-generation printable electronics.
46 Towards this end, a conductive graphene ink was prepared by dispersing EG flakes in DMF with
47 a high concentration (10 mg/mL; Fig. 7a). Application of the as-prepared graphene ink on A4-
48 size paper using a paintbrush (Fig. 7b) easily transformed the paper into an electrically
49 conductive sheet. The bonding of cellulose fiber in paper produces many air passages or pores
50
51
52
53
54
55
56
57
58
59
60

1
2
3 throughout the paper (Fig. S16a). Thus, the highly porous nature of paper provides a strong
4
5 capillary force for the EG ink, enhancing solvent absorption and leading to a conformal coating
6
7 of EG ink on paper (Fig. S16b). Moreover, a simple film adhesion test with a piece of cellophane
8
9 tape demonstrated strong adhesion between the EG and paper, confirming high film stability
10
11 against damage, such as scratching or peeling off (Fig. 7c). Figure 7d presents the relationship
12
13 between the paper resistance and the amount of EG loading (in mg cm^{-2}). A sheet resistance of
14
15 $\sim 11 \Omega \text{ sq.}^{-1}$ was obtained with an EG loading of 0.74 mg cm^{-2} , comparable to carbon nanotube
16
17 paper.³⁶ Moreover, the graphene paper possessed excellent mechanical properties since after
18
19 bending to a 4-mm radius, there was no significant change in electrical conductivity (Fig. 7e).

20
21 To demonstrate the multifunction of the EG paper, we explored the potential of EG-coated
22
23 paper for all solid-state flexible supercapacitors. For this purpose, a polyvinyl alcohol/ H_2SO_4 gel
24
25 was drop-cast onto the top surface of EG-coated paper (with a loading of $\sim 0.60 \text{ mg cm}^{-2}$) and
26
27 solidified overnight. Afterwards, two pieces of EG paper electrodes were integrated into an all-
28
29 solid-state supercapacitor without using an additional current collector (Fig. 8a). The
30
31 electrochemical properties of the as-fabricated device were investigated by cyclic voltammetry.
32
33 The binder- and additive-free fabricated EG paper-based supercapacitor exhibited typical double-
34
35 layer capacitive behaviour at various scan rates (Fig. 8b and S17a). The area capacitance of the
36
37 flexible EG paper supercapacitor was $\sim 11.3 \text{ mF cm}^{-2}$ at a low scan rate of 1 mV s^{-1} (Fig. 8d),
38
39 comparable to or even higher than thin-film rGO or carbon nanotubes on flexible substrates.^{37,38}
40
41 In addition, the gravimetric capacitance calculated based on the area capacitance ranges from
42
43 18.8 to 56.6 F g^{-1} , depending of the loading of EG on paper varying from 0.6 to 0.2 mg cm^{-2} ,
44
45 respectively (Fig. S17). Remarkably, the device exhibited high rate capability that could be
46
47
48
49
50
51
52
53
54
55
56
57
58
59
60

1
2
3 operated up to 5000 mV s⁻¹ (Fig. 8c). The rate capability achieved in this work was thus superior
4
5 to that of carbon nanotubes and/or rGO-coated cellulose paper supercapacitors.^{37,39-42}
6
7
8
9

10 **CONCLUSION:**

11
12 Taken together, our electrochemical exfoliation of graphite in aqueous sulphate salt
13 electrolyte solution effectively reduces the oxidation degree and thereby significantly improves
14 the chemical and electronic properties of graphene. Thin-layer graphene sheets were obtained at
15 a high yield with large flake size and can be produced on a scale of tens of grams, demonstrating
16 the great potential for industrial scale-up production. The EG has the highest C/O ratio (17.2)
17 and hole mobility (~ 310 cm² V⁻¹ s⁻¹) among all the reported values of EG obtained in acidic
18 electrolytes and solution-processed rGO. The solution-processability of high-quality EG in
19 organic solvents permits their direct use in transparent films and conductive ink, providing great
20 advantage for the fabrication of graphene-based materials and devices. Low-cost and
21 environmentally-friendly production of such high-quality graphene is important, not only for
22 future generation electronics but also for large-scale applications, such as composite materials,
23 supercapacitors, fuel-cells, and batteries.
24
25
26
27
28
29
30
31
32
33
34
35
36
37
38
39
40
41
42

43 *Acknowledgement:* This work was financially supported by ERCF grants on NANOGRAPH and
44 2DMATER, DFG Priority Program SPP 1459, EU Project GENIUS, MOLESOL and EC under
45 Graphene Flagship (No. CNECT-ICT-604391).
46
47
48
49
50

51 *Supporting Information Available:* Experimental details, photographs of electrochemical
52 exfoliation in large-scale and in different electrolyte systems, AFM, HRTEM and optical
53 microscopic images, XPS, solid-state NMR spectra and XRD of EG; AFM image of EG FET
54
55
56
57
58
59
60

1
2
3 device, UV-Vis and sheet resistance of EG thin film before and after acid doping; SEM image of
4
5 EG coated paper and electrochemical characterizations of EG paper based supercapacitors;
6
7
8 summary of electrochemical exfoliation in different inorganic salts and comparison of elemental
9
10 analysis and mobility of EG with different types of graphene. This material is available free of
11
12 charge *via* the Internet at <http://pubs.acs.org>.
13
14
15
16
17
18

19 REFERENCES

- 20
21
22 (1) Wang, Y.; Chen, X.; Zhong, Y.; Zhu, F.; Loh, K. P. *Appl. Phys. Lett.* **2009**, *95*, 063302.
23
24 (2) Bae, S.; Kim, H.; Lee, Y.; Xu, X. F.; Park, J. S.; Zheng, Y.; Balakrishnan, J.; Lei, T.; Kim,
25
26 H. R.; Song, Y. I.; Kim, Y. J.; Kim, K. S.; Ozyilmaz, B.; Ahn, J. H.; Hong, B. H.; Iijima, S.
27
28 *Nat. Nanotechnol.* **2010**, *5*, 574.
29
30 (3) Wu, D. Q.; Zhang, F.; Liang, H. W.; Feng, X. L. *Chem. Soc. Rev.* **2012**, *41*, 6160.
31
32 (4) Parvez, K.; Yang, S. B.; Hernandez, Y.; Winter, A.; Turchanin, A.; Feng, X. L.; Müllen, K.
33
34 *ACS Nano* **2012**, *6*, 9541.
35
36 (5) Wu, Z. S.; Parvez, K.; Feng, X.; Müllen, K. *Nat. Commun.* **2013**, *4*, 2487.
37
38 (6) Geim, A. K.; Novoselov, K. S. *Nat. Mater.* **2007**, *6*, 183.
39
40 (7) Park, S.; Ruoff, R. S. *Nat. Nanotechnol.* **2009**, *4*, 217.
41
42 (8) Novoselov, K. S.; Geim, A. K.; Morozov, S. V.; Jiang, D.; Zhang, Y.; Dubonos, S. V.;
43
44 Grigorieva, I. V.; Firsov, A. A. *Science* **2004**, *306*, 666.
45
46 (9) Sutter, P. W.; Flege, J. I.; Sutter, E. A. *Nat. Mater.* **2008**, *7*, 406.
47
48 (10) Lee, Y.; Bae, S.; Jang, H.; Jang, S.; Zhu, S. E.; Sim, S. H.; Song, Y. I.; Hong, B. H.; Ahn,
49
50 J. H. *Nano Lett.* **2010**, *10*, 490.
51
52
53
54
55
56
57
58
59
60

- 1
2
3
4
5
6
7
8
9
10
11
12
13
14
15
16
17
18
19
20
21
22
23
24
25
26
27
28
29
30
31
32
33
34
35
36
37
38
39
40
41
42
43
44
45
46
47
48
49
50
51
52
53
54
55
56
57
58
59
60
- (11) Eda, G.; Fanchini, G.; Chhowalla, M. *Nat. Nanotechnol.* **2008**, *3*, 270.
- (12) Hernandez, Y.; Nicolosi, V.; Lotya, M.; Blighe, F. M.; Sun, Z. Y.; De, S.; McGovern, I. T.; Holland, B.; Byrne, M.; Gun'ko, Y. K.; Boland, J. J.; Niraj, P.; Duesberg, G.; Krishnamurthy, S.; Goodhue, R.; Hutchison, J.; Scardaci, V.; Ferrari, A. C.; Coleman, J. N. *Nat. Nanotechnol.* **2008**, *3*, 563.
- (13) Wang, J. Z.; Manga, K. K.; Bao, Q. L.; Loh, K. P. *J. Am. Chem. Soc.* **2011**, *133*, 8888.
- (14) Shih, C. J.; Vijayaraghavan, A.; Krishnan, R.; Sharma, R.; Han, J. H.; Ham, M. H.; Jin, Z.; Lin, S. C.; Paulus, G. L. C.; Reuel, N. F.; Wang, Q. H.; Blankschtein, D.; Strano, M. S. *Nat. Nanotechnol.* **2011**, *6*, 439.
- (15) Parvez, K.; Li, R. J.; Puniredd, S. R.; Hernandez, Y.; Hinkel, F.; Wang, S. H.; Feng, X. L.; Müllen, K. *ACS Nano* **2013**, *7*, 3598.
- (16) Lee, J. H.; Shin, D. W.; Makotchenko, V. G.; Nazarov, A. S.; Fedorov, V. E.; Kim, Y. H.; Choi, J. Y.; Kim, J. M.; Yoo, J. B. *Adv. Mater.* **2009**, *21*, 4383.
- (17) Liu, N.; Luo, F.; Wu, H. X.; Liu, Y. H.; Zhang, C.; Chen, J. *Adv. Funct. Mater.* **2008**, *18*, 1518.
- (18) Su, C. Y.; Lu, A. Y.; Xu, Y. P.; Chen, F. R.; Khlobystov, A. N.; Li, L. J. *ACS Nano* **2011**, *5*, 2332.
- (19) Lu, J.; Yang, J. X.; Wang, J. Z.; Lim, A. L.; Wang, S.; Loh, K. P. *ACS Nano* **2009**, *3*, 2367.
- (20) Liu, J. L.; Yang, H. P.; Zhen, S. G.; Poh, C. K.; Chaurasia, A.; Luo, J. S.; Wu, X. Y.; Yeow, E. K. L.; Sahoo, N. G.; Lin, J. Y.; Shen, Z. X. *Rsc. Adv.* **2013**, *3*, 11745.
- (21) Shang, N. G.; Papakonstantinou, P.; Sharma, S.; Lubarsky, G.; Li, M. X.; McNeill, D. W.; Quinn, A. J.; Zhou, W. Z.; Blackley, R. *Chem. Commun.* **2012**, *48*, 1877.
- (22) Beck, F.; Jiang, J.; Krohn, H. *J Electroanal. Chem.* **1995**, *389*, 161.

- 1
2
3
4 (23) Beck, F.; Junge, H.; Krohn, H. *Electrochim. Acta* **1981**, *26*, 799.
5
6 (24) Goss, C. A.; Brumfield, J. C.; Irene, E. A.; Murray, R. W. *Anal. Chem.* **1993**, *65*, 1378.
7
8 (25) Cheng, Z. G.; Zhou, Q. Y.; Wang, C. X.; Li, Q. A.; Wang, C.; Fang, Y. *Nano Lett.* **2011**,
9
10 *11*, 767.
11
12 (26) Sun, Z. Z.; Yan, Z.; Yao, J.; Beitler, E.; Zhu, Y.; Tour, J. M. *Nature* **2010**, *468*, 549.
13
14 (27) Yu, Q. K.; Jauregui, L. A.; Wu, W.; Colby, R.; Tian, J. F.; Su, Z. H.; Cao, H. L.; Liu, Z.
15
16 H.; Pandey, D.; Wei, D. G.; Chung, T. F.; Peng, P.; Guisinger, N. P.; Stach, E. A.; Bao, J.
17
18 M.; Pei, S. S.; Chen, Y. P. *Nat. Mater.* **2011**, *10*, 443.
19
20 (28) Malard, L. M.; Pimenta, M. A.; Dresselhaus, G.; Dresselhaus, M. S. *Phys. Rep.* **2009**, *473*,
21
22 51.
23
24 (29) Ferrari, A. C.; Meyer, J. C.; Scardaci, V.; Casiraghi, C.; Lazzeri, M.; Mauri, F.; Piscanec,
25
26 S.; Jiang, D.; Novoselov, K. S.; Roth, S.; Geim, A. K. *Phys. Rev. Lett.* **2006**, *97*, 187401.
27
28 (30) Buglione, L.; Chng, E. L. K.; Ambrosi, A.; Sofer, Z.; Pumera, M. *Electrochem. Commun.*
29
30 **2012**, *14*, 5.
31
32 (31) Feng, H.; Cheng, R.; Zhao, X.; Duan, X.; Li, J. *Nat. Commun.* **2013**, *4*, 1539.
33
34 (32) Moon, I. K.; Lee, J.; Ruoff, R. S.; Lee, H. *Nat. Commun.* **2010**, *1*, 73.
35
36 (33) Shin, H. J.; Choi, W. M.; Choi, D.; Han, G. H.; Yoon, S. M.; Park, H. K.; Kim, S. W.; Jin,
37
38 Y. W.; Lee, S. Y.; Kim, J. M.; Choi, J. Y.; Lee, Y. H. *J. Am. Chem. Soc.* **2010**, *132*, 15603.
39
40 (34) Li, S. S.; Tu, K. H.; Lin, C. C.; Chen, C. W.; Chhowalla, M. *ACS Nano* **2010**, *4*, 3169.
41
42 (35) Kholmanov, I. N.; Magnuson, C. W.; Aliev, A. E.; Li, H. F.; Zhang, B.; Suk, J. W.; Zhang,
43
44 L. L.; Peng, E.; Mousavi, S. H.; Khanikaev, A. B.; Piner, R.; Shvets, G.; Ruoff, R. S.
45
46 *Nano Lett.* **2012**, *12*, 5679.
47
48
49
50
51
52
53
54
55
56
57
58
59
60

- 1
2
3
4
5
6
7
8
9
10
11
12
13
14
15
16
17
18
19
20
21
22
23
24
25
26
27
28
29
30
31
32
33
34
35
36
37
38
39
40
41
42
43
44
45
46
47
48
49
50
51
52
53
54
55
56
57
58
59
60
- (36) Hu, L.; Choi, J. W.; Yang, Y.; Jeong, S.; La Mantia, F.; Cui, L. F.; Cui, Y. *Proc. Natl. Acad. Sci. USA* **2009**, *106*, 21490.
- (37) Yoo, J. J.; Balakrishnan, K.; Huang, J. S.; Meunier, V.; Sumpter, B. G.; Srivastava, A.; Conway, M.; Reddy, A. L. M.; Yu, J.; Vajtai, R.; Ajayan, P. M. *Nano Lett* **2011**, *11*, 1423.
- (38) Kaempgen, M.; Chan, C. K.; Ma, J.; Cui, Y.; Gruner, G. *Nano Lett* **2009**, *9*, 1872.
- (39) Hu, S.; Rajamani, R.; Yu, X. *Appl. Phys. Lett.* **2012**, *100*, 104103.
- (40) Weng, Z.; Su, Y.; Wang, D. W.; Li, F.; Du, J. H.; Cheng, H. M. *Adv. Energy. Mater.* **2011**, *1*, 917.
- (41) Kang, Y. J.; Chun, S. J.; Lee, S. S.; Kim, B. Y.; Kim, J. H.; Chung, H.; Lee, S. Y.; Kim, W. *ACS Nano* **2012**, *6*, 6400.
- (42) Kang, Y. J.; Chung, H.; Han, C. H.; Kim, W. *Nanotechnology* **2012**, *23*, 065401.

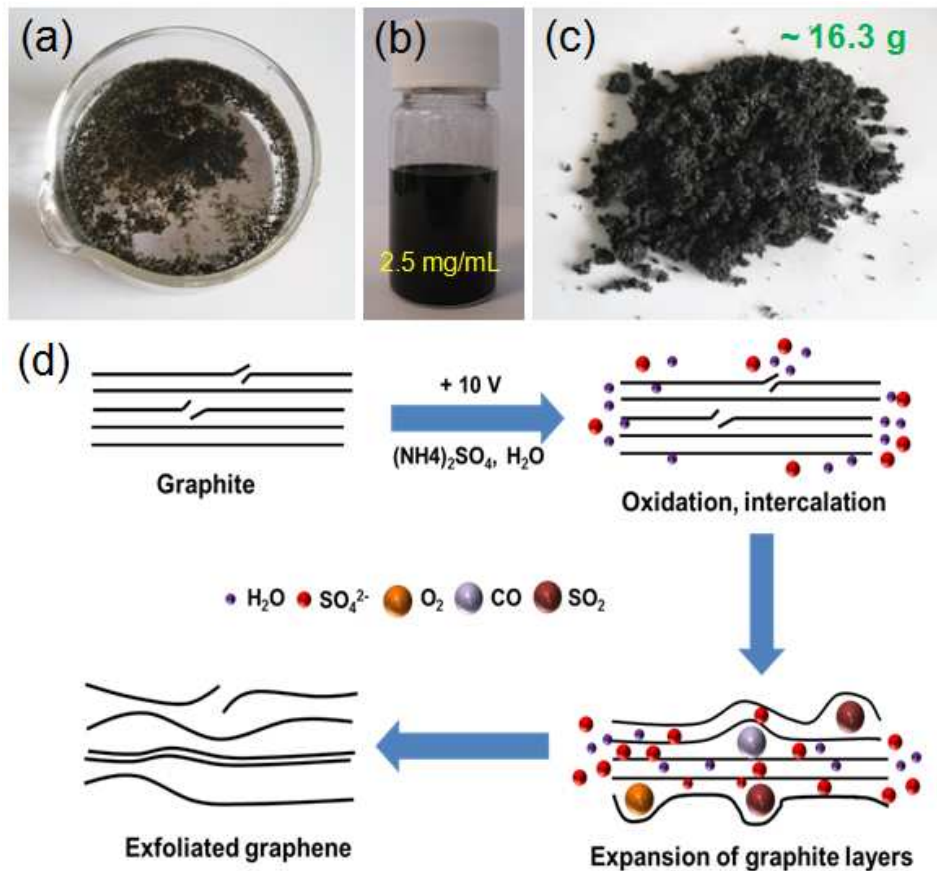


Figure 1. Photograph of (a) graphite flakes after electrochemical exfoliation, (b) dispersed EG in DMF solution (concentration ~ 2.5 mg/mL), (c) EG powders in a bulk scale (~ 16.3 g). (d) Schematic illustration of the mechanism of electrochemical exfoliation.

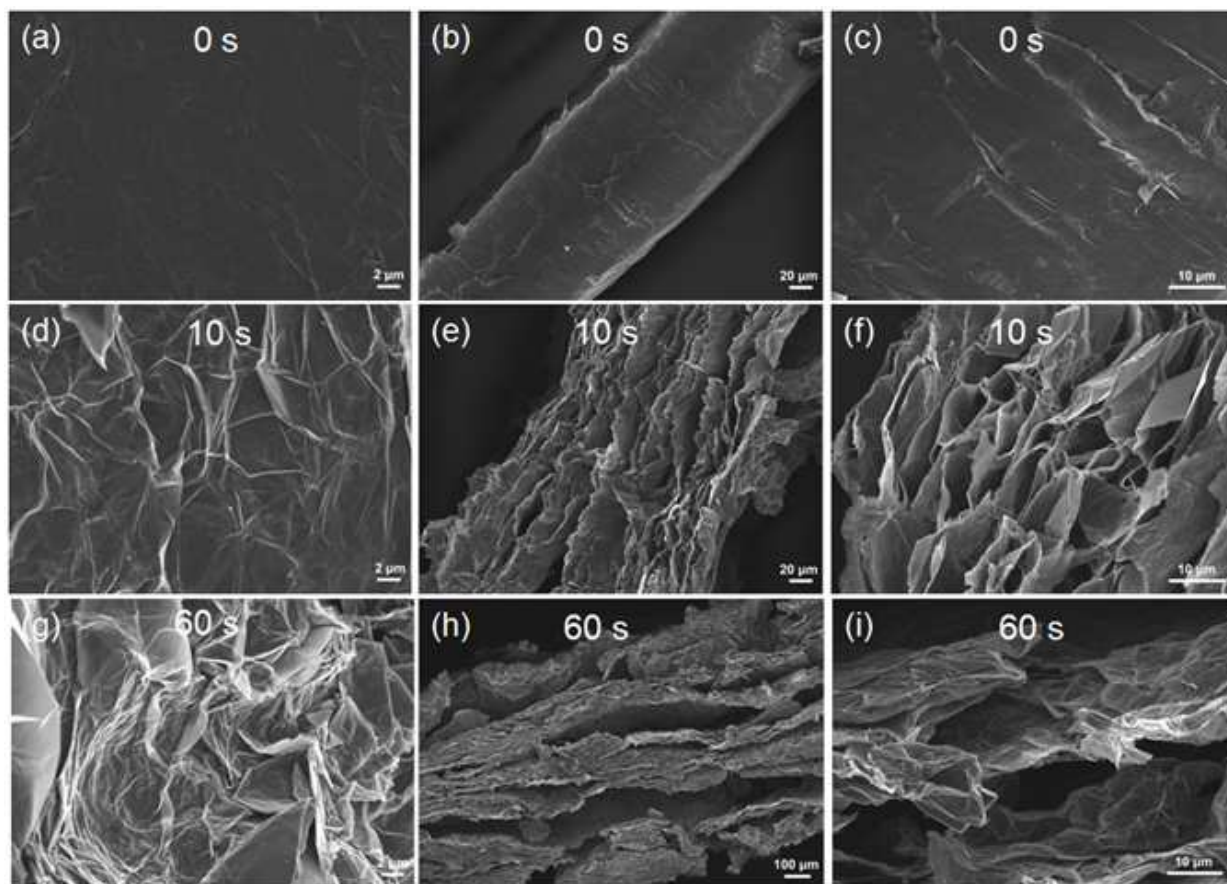


Figure 2. SEM images of (a), (d), and (g) surface and (b), (e), and (h) edge morphology of the graphite foil after applying a bias voltage of +10 V for 0 s, 10 s, and 60 s in aqueous $(\text{NH}_4)_2\text{SO}_4$ electrolyte solution, respectively. (c), (f), and (i) are magnified images of (b), (e), and (h), respectively.

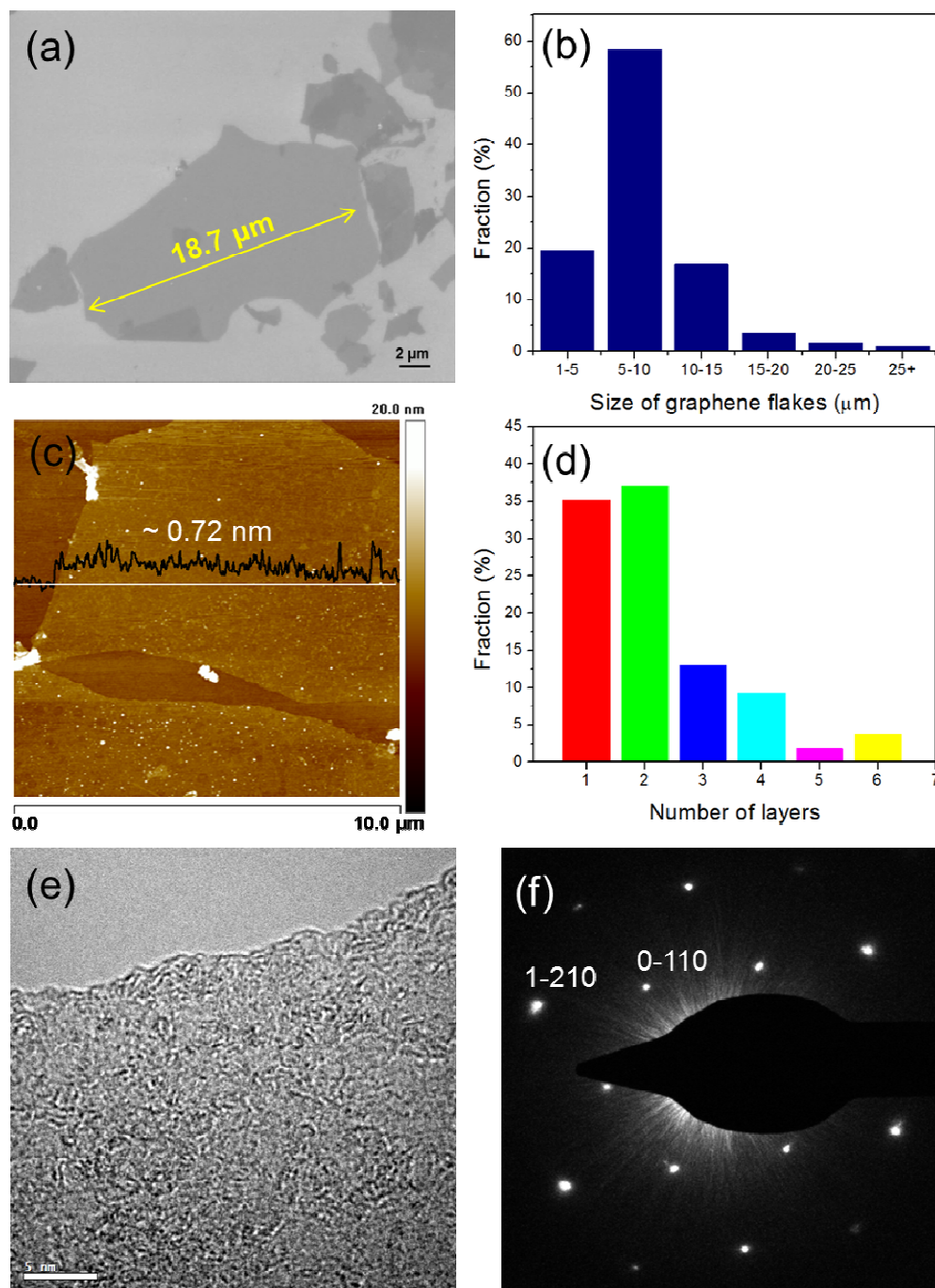


Figure 3. (a) SEM image of EG, (b) statistical flake size analysis of graphene sheets by SEM. (c) AFM image of EG on silicon substrate, (d) statistical thickness analysis of EG by AFM. (e) HRTEM of single-layer graphene. (f) SAED pattern of EG.

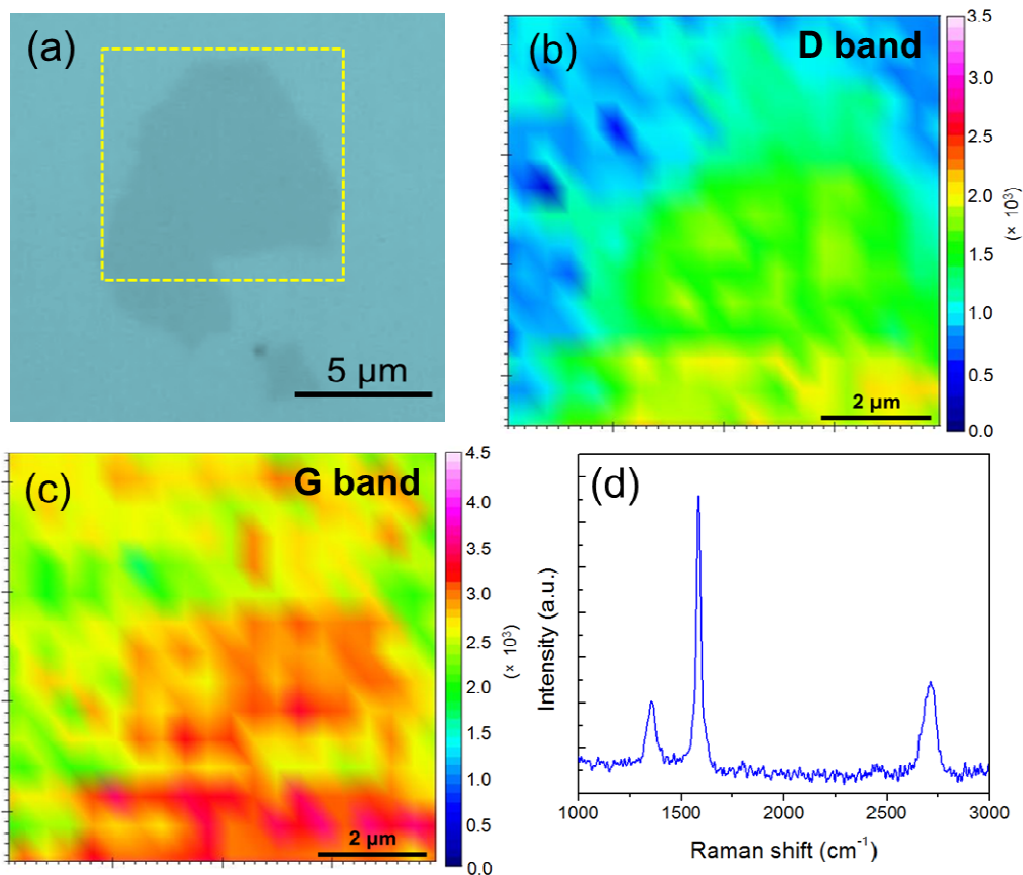


Figure 4. (a) Optical microscopic image of an EG flake. Scale bar 5 μm . (b) and (c) Raman intensity maps for D and G peak, respectively. (d) Representative Raman spectra. The Raman excitation laser wavelength is 532 nm.

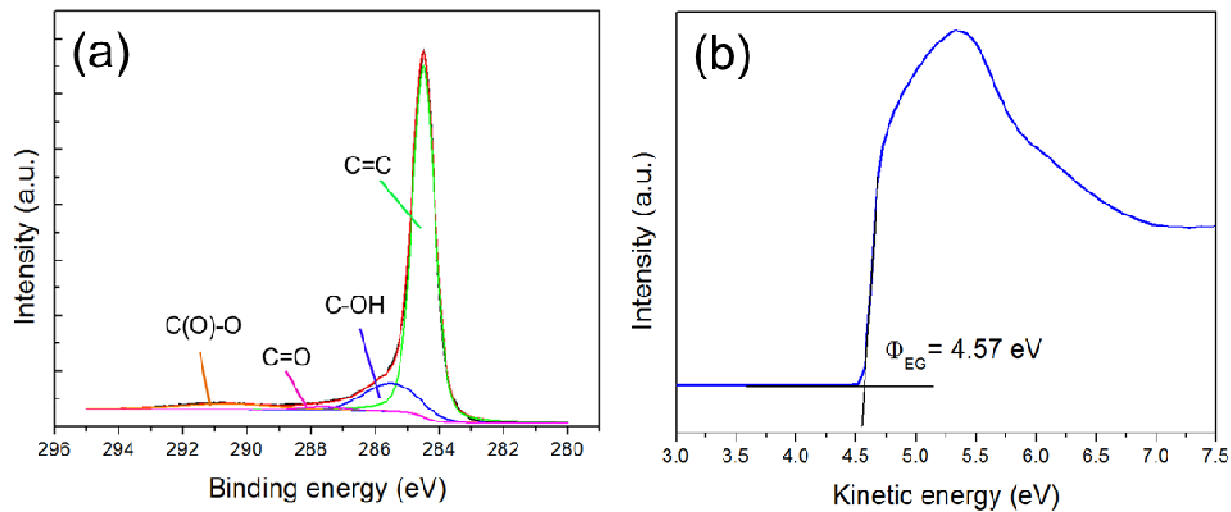


Figure 5. (a) XPS C1s spectra of EG. (b) The secondary electron cut-off of EG measured from ultraviolet photoemission spectra.

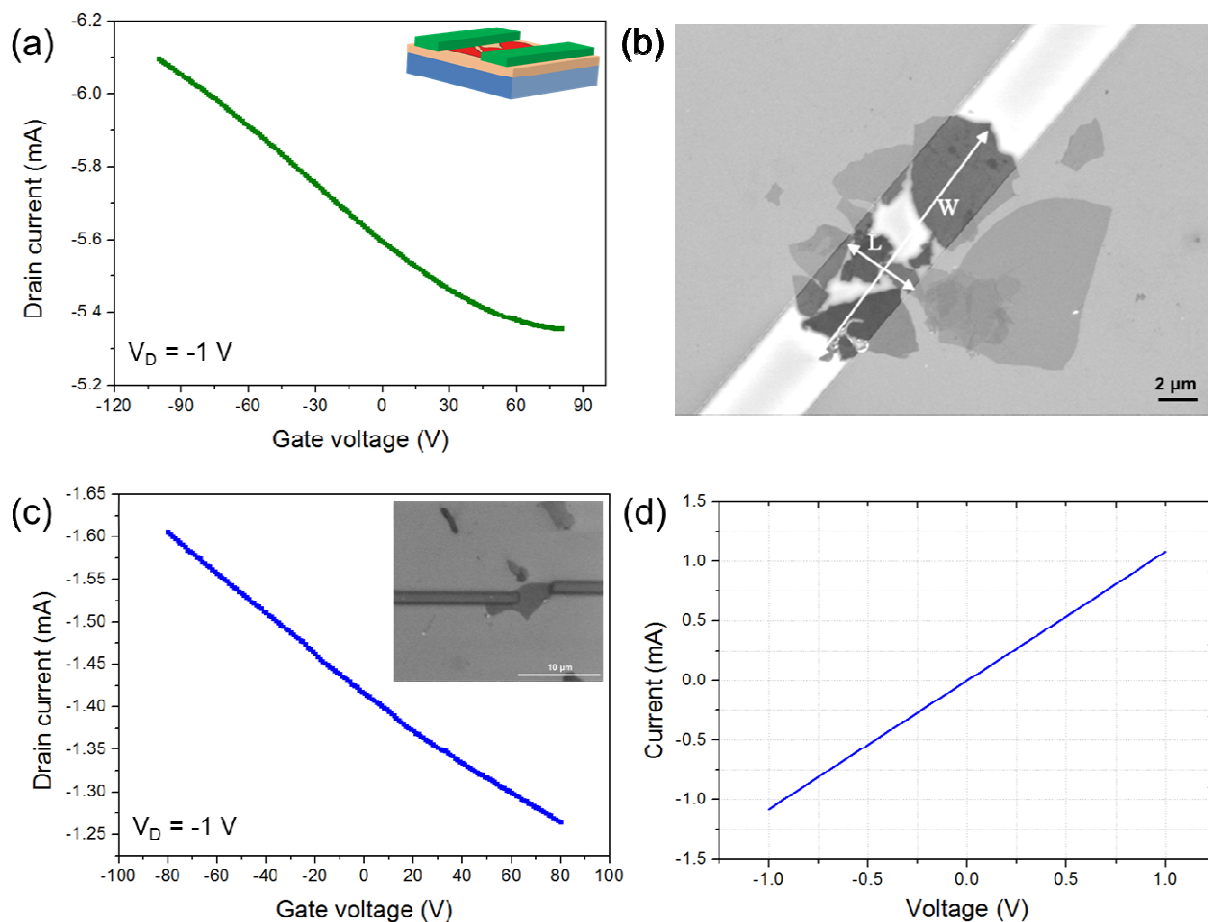


Figure 6. (a) Transfer curve for a FET device based on EG thin film. (b) SEM image of the fabricated device showing thin EG flakes between the Au electrodes. Channel length and width are indicated by arrows. (c) Transfer curve of an FET device based on single-layer EG (inset is the SEM image of the fabricated device). (d) Current-voltage (I - V) curve of an isolated single-layer EG flake.

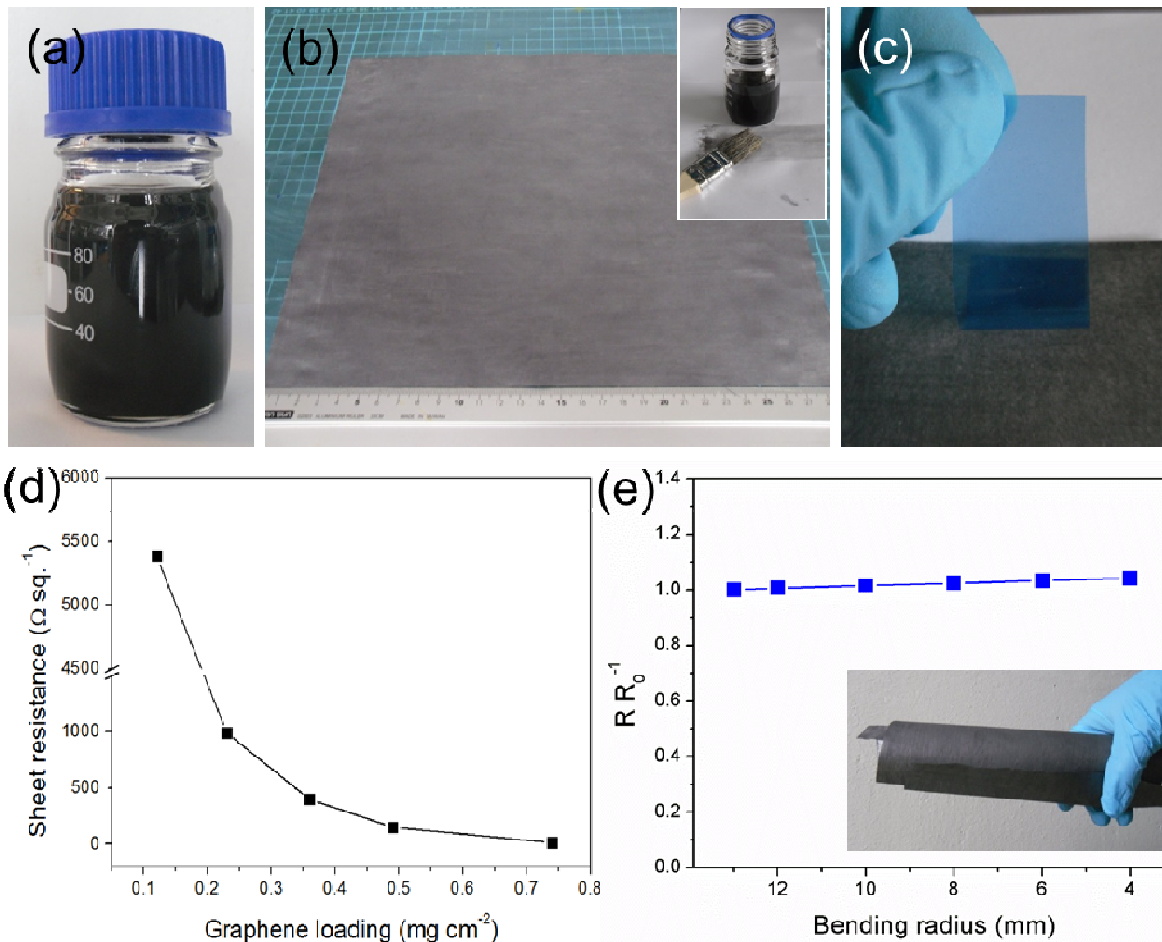


Figure 7. (a) Photograph of EG in DMF (10 mg/mL) used as an ink; (b) commercial A4-size paper coated with EG using a paintbrush (inset). (c) Film adhesion test with cellophane tape (d) Relationship between the resistances of the paper with graphene loading. (e) Changes in sheet resistance after bending the conductive paper into different radii.

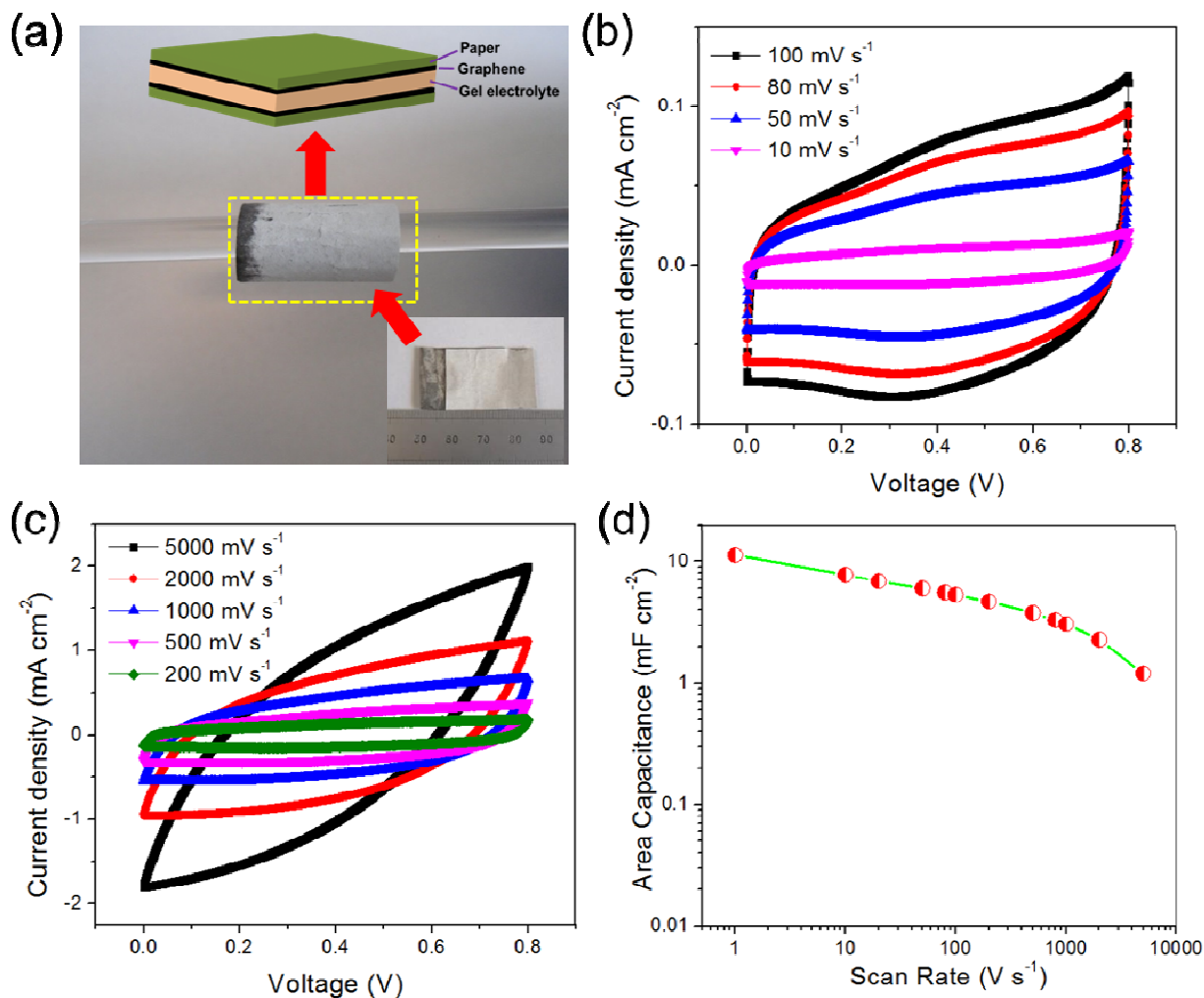
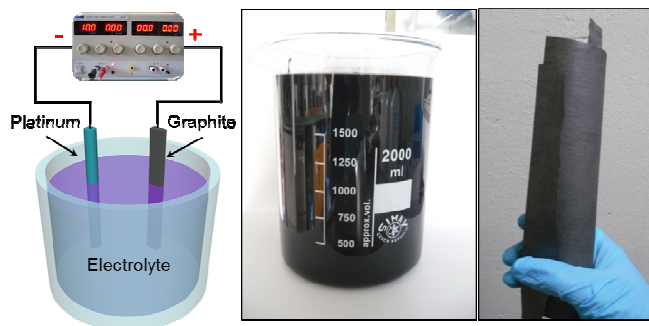


Figure 8. (a) Photographs of supercapacitor based on EG ink-coated paper, where the device is rolled around a glass rod. Inset shows a photograph of the device prior to rolling. (b) and (c) Cyclic voltammetry curves of EG paper based supercapacitor (loading 0.6 mg cm^{-2}) at a scan rates from 10 to 100 mV s^{-1} and 200 to 5000 mV s^{-1} , respectively. (d) Evolution of area capacitance versus scan rate.

TOC image



1
2
3
4
5
6
7
8
9
10
11
12
13
14
15
16
17
18
19
20
21
22
23
24
25
26
27
28
29
30
31
32
33
34
35
36
37
38
39
40
41
42
43
44
45
46
47
48
49
50
51
52
53
54
55
56
57
58
59
60